Analytical Harmonic Method for Modeling High-Frequency Oscillation With Applications to Aircraft Piston Pump Vibration Analysis

Lei Li, Kok-Meng Lee, *Fellow, IEEE*, Xiaoping Ouyang, and Huayong Yang

***Abstract*—Undesired oscillations are often encountered in controlled systems at steady state due to high-frequency (HF) periodic disturbance and/or feedback noises. This article presents a computationally efficient alternative to derive an analytical harmonic model (AHM) that expresses the oscillatory variable as a series of harmonic kernel vectors and a position-independent harmonic amplitude vector for identifying the dominant harmonic components of the undesired effects on the manipulated variables. Illustrated in the context of an aircraft pressure-controlled piston pump (PC-PP) where the pressure feedback pulsations and the torque disturbances from the piston/slipper assemblies lead to HF swash-plate (SP) oscillation at steady state, the AHM and its significance were investigated experimentally on a PC-PP test-rig capable of simultaneously measuring the HF feedback pressure and SP-angle. Good agreements between the experimental and numerical results validate the AHM, and reveal that the HF SP-oscillation is dominated by its fundamental harmonic component, and primarily contributed by the disturbance torque.**

***Index Terms*—Analytical harmonic model (AHM), feedback noises, piston pump, swash-plate oscillation, vibration analysis.**

I. Introduction

SUSTAINED steady-state high-frequency (HF) oscillations that occur in controlled systems are undesired as they cause increased vibration and wear/tear leading to device damage. Repetitive time-varying excitations and/or disturbances are commonly encountered in continuous operations [1]–[6] of mechanical and electrical devices; for example, electromagnetic actuators excited by current harmonics [3], [4], [6], piston-pumps where chamber pressures are subjected to repetitive transitions between high discharge and low suction pressures [7], to name a few. The repetitive excitation and disturbances along with their accompanying periodic oscillations offer rich structured information for inspecting the underlying dynamics and for evaluating the performance of these industrial devices. To provide a basis for performance monitoring and/or ripple suppression [1]–[6], the periodic oscillations and their effects on the involved dynamic systems must be analyzed and identified in a computationally efficient manner by properly accounting for the structured information, especially for safety-critical applications (like aircraft piston pumps or other devices requiring uninterruptable operations).

In aircraft piston-pumps, the discharge pressure is regulated by an efficient swash-plate (SP) angle manipulation [8], [9] through a pressure-controlled (PC) system; and once appropriately manipulated, the SP-angle (as a manipulated variable) is expected to maintain at a steady-state value. However, repetitive transitions between high and low pressures of the piston chamber result in HF oscillations. Furthermore, the inherent HF feedback (discharge-pressure) ripples [10], [11] in the PC system, along with the pulsating torque disturbances [12]–[14], cause the SP-angle to oscillate at HF about its steady-state position [15], [16], which incur larger structural-borne noises [17], poor efficiency [18], and even device damage. Due to the complex and/or nonlinear dynamics involved in the PC system of the aircraft pressure-controlled piston pump (PC-PP), it is difficult to relate the resulting SP oscillations explicitly to the periodic torque disturbance and feedback pressure ripples. Motivated by the needs to analyze/predict SP oscillations of an aircraft PC-PP, this article presents an analytical method to derive computationally efficient models that directly relate the HF vibration characteristics as a function of feedback ripples and pulsating disturbances by actively utilizing the periodic information and properly formulating the dynamic model; both time- and frequency-domain formulations are discussed.

Noting that early models assuming a constant SP-angle and/or an averaged disturbance torque may be inaccurate, Dobchuk [19] modeled the internal dynamics of the pump at the subcomponent level and computed the SP-angle variations; however, due to

Manuscript received April 3, 2020; revised June 19, 2020; accepted July 21, 2020. Date of publication July 28, 2020; date of current version April 15, 2021. This work was supported in part by the National Science Foundation of China under Grant 51675473, in part by U.S. National Science Foundation under Grant CMMI-1662700, and in part by the National Basic Research Program of China (973 Program) under Grant 2013CB035803. Recommended by Technical Editor L. Zhu and Senior Editor Y. Li. *(Corresponding author: Kok-Meng Lee.)*

Lei Li, Xiaoping Ouyang, and Huayong Yang are with the State Key Lab of Fluid Power and Mechatronics Systems, Zhejiang University, Hangzhou 310027, China (e-mail: tjull1991@163.com; ouyangxp@zju.edu.cn; yhy@zju.edu.cn).

Kok-Meng Lee is with the Woodruff School of Mechanical Engineering, Georgia Institute of Technology, Atlanta, GA 30332 USA (e-mail: kokmeng.lee@me.gatech.edu).

Color versions of one or more of the figures in this article are available online at https://ieeexplore.ieee.org.

Digital Object Identifier 10.1109/TMECH.2020.3012297

limited angle-sensor resolution, the measured SP-angle was a sequence of discrete signals with a step size larger than the SP oscillation amplitude. In [20], the vibration of a constant power-regulated PP was analyzed numerically; simulations showed that the SP-angle and its control-valve displacement oscillated periodically at steady state. In [15] and [21], the HF behaviors of a floating-cup pump were investigated with the SP-angle measured by an inductive sensor. Their experimental results revealed that the periodic SP oscillation has a fundamental frequency equaling to the product of pump speed and piston-number (with its amplitude increasing with the discharge pressure and decreasing with the pump speed up to 3000 r/min), and that the pump volumetric discharge has no impact on the swash plate oscillation. Similar investigation was conducted in [13] for a variable displacement-PP numerically demonstrating the effects of the valve-plate design and pump speed (up to 3000 r/min) on SP oscillations. More recently, a frequency-domain model for numerical investigating the effects of PC parameters on the HF SP oscillations was experimentally validated with measured SP-angle and discharge pressure in [16].

Due to the complexity and nonlinearity involved in the PC-PP dynamics, analytical characterization of the HF oscillations under various pump speeds at steady state remains a challenge. Conventional time-domain models (TDMs) [19]–[21] are commonly formulated as a set of nonlinear differential equations (that require highly repetitive time-consuming integrations) to calculate the point-by-point HF oscillations, whereas complex calculations are necessary to convert frequency-domain results into time-domain counterparts in the recently developed frequency model [16]. These existing (time and frequency) methods, in general, focus on describing the complex (high-order) and/or nonlinear system dynamics without exploiting the structured information in periodic oscillations. Although periodicities of HF discharge-pressure ripples [10], [11] and pulsating torque disturbances [12]–[14] as well as their resulting effects on the SP-angle [15], [16], [20], are well known in the field of fluid-power, there has been scarcely any published work that exploits their harmonics in the modeling of piston pumps. This article offers a novel method, referred to here as analytical harmonic model (AHM), to derive explicit relationships among the harmonics of key performance variables. Specifically, AHM simultaneously offers both time- and frequency-domain information for analyses, and explicitly characterizes the harmonics of the periodic oscillations as a function of feedback pressure ripples and pulsating external disturbance. As a result, time-consuming calculations that are required in existing (time- and frequency domain) methods are avoided in the rest offered here as a computationally efficient alternative. The remainder of this article is organized as follows.

1) Section II begins with the derivation of AHM that expresses the oscillatory variable as a series of harmonic kernel vectors and a position-independent harmonic amplitude vector. Its significances as a computationally efficient alternative to identify the dominant harmonic components of the undesired effects on the manipulated variables are then illustrated in the context of a high-order stable controlled PC-PP system.
2) Section III presents the investigations conducted on an aircraft PC-PP, both in time and frequency domain under typical operating speeds, which illustrate and validate the AHM, and provide physical insights into the characteristics of the HF SP oscillations under various speeds.

II. Analytical Harmonic Model

For a noisy control system suffered from HF periodic external disturbances and/or feedback signal noises, the controlled or manipulated variable may oscillate periodically at steady state. As an illustration, consider a rotational dynamic system, where x represents a function of its angular position $\theta(t) = \theta(t = 0) + \omega t$; and ω is the operating frequency. The periodic position-dependent variable x is an incremental change from its steady-state value x_0; and its first and second time-derivatives can be expressed as a series of *harmonic kernel vectors* $\mathbf{h}(\ell\theta)$, where $\ell = 0, 1, 2, \ldots$, and a position-independent *harmonic amplitude vector* (HAV) $\mathbf{x}_\ell$ with amplitude x_ℓ and phase angle $\varphi_{x\ell}$

$$x(\theta) = \sum_{\ell=1,2\ldots}^{\infty} \mathbf{h}(\ell\theta)\,\mathbf{x}_\ell \tag{1a}$$

$$\dot{x}(\theta) = \frac{dx}{dt} = \omega \sum_{\ell=1,2\ldots}^{\infty} \ell\mathbf{h}(\ell\theta)\mathbf{S}\mathbf{x}_\ell \tag{1b}$$

$$\ddot{x}(\theta) = \frac{d^2x}{dt^2} = -\omega^2 \sum_{\ell=1,2\ldots}^{\infty} \ell^2\mathbf{h}(\ell\theta)\,\mathbf{x}_\ell \tag{1c}$$

where

$$\mathbf{h}(.) = \left[\sin(.)\ \cos(.)\right];\ \frac{\mathbf{x}_\ell}{x_\ell} = \begin{bmatrix}\cos\varphi_{x\ell}\\ \sin\varphi_{x\ell}\end{bmatrix} \text{ and } \mathbf{S} = \begin{bmatrix}0 & -1\\ 1 & 0\end{bmatrix} \tag{1d–f}$$

The trigonometric functions in (1d) obey the orthogonal property [22]

$$\sum_{n=1}^{N} \mathbf{h}\left[k\left(\theta_1 + 2\pi(n-1)/N\right)\right] = \begin{cases} N\mathbf{h}(\ell N\theta_1) & k = \ell N\\ \mathbf{0} & \text{others.}\end{cases} \tag{1g}$$

As defined in (1a–g), the dominant harmonic components of the periodic pulsating variables and their effects on the noisy dynamic system can be fully characterized by the position-independent HAVs in terms of the operating frequency ω.

Given a physics-based dynamic model, the HAVs can be derived for its periodic external disturbance $\mathbf{D}_\ell$, feedback noise $\mathbf{Y}_\ell$ and the controlled variable ripples $\mathbf{C}_\ell$ using the harmonic formulation (1a–c)

$$\mathbf{C}_\ell = \mathbf{G}(\omega)\,\mathbf{D}_\ell - \mathbf{H}(\omega)\,\mathbf{Y}_\ell. \tag{2}$$

In (2), where the minus sign originates from the negative feedback, $\mathbf{G}(\omega)$ and $\mathbf{H}(\omega)$ account for the dynamics of the disturbance and feedback, respectively. Equation (2) is referred to here as the position-independent AHM, which offers an efficient means to analyze the dynamic effects of the disturbance $\mathbf{D}_\ell$ on the controlled variable $\mathbf{C}_\ell$ based on the measured $\mathbf{Y}_\ell$. The time- and frequency-domain dynamics are simultaneously accounted for

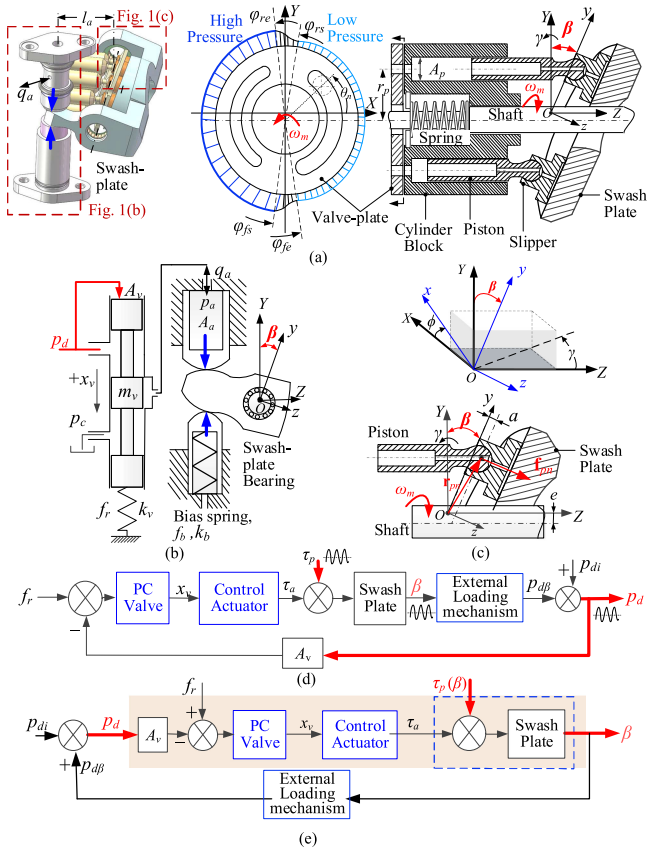

Fig. 1. PC-PP system. (a) CAD model. (b) SP adjustment mechanism. (c) Piston/slipper (P/S) assembly and coordinate systems. (d) PC system. (e) SP angle as the system output.

using (1a) and the AHM (2), which go beyond the conventional analytical methods based on Laplace-transform or numerical integration operations. AHM can be applied to a broad range of applications where periodic disturbances and/or feedback noises on the controlled variable are major concerns. As illustrated in Appendix B, where a noisy speed control system is formulated, AHM once derived can be used as constraints to design an appropriate controller to suppress ripples.

A. Pressure Controlled Piston Pump

The method to derive an AHM in terms of the HAVs ($\mathbf{D}_\ell$ and $\mathbf{C}_\ell$) of a high-order stable controlled system at steady state is illustrated in the context of a PC-PP system (see Fig. 1). In a PC-PP, the rotation of the shaft/cylinder-block (driven by an electric motor operating at speed ω_m) is converted into the reciprocating displacement of the piston-slipper assemblies pressing against an inclined SP. As schematically shown in Fig. 1(a), the inclined SP of a typical PC-PP is subjected to the torques from the vertical actuator [23] [see Fig. 1(b)], and N evenly distributed piston/slipper (P/S) assemblies [see Fig. 1(c)]. The two block diagrams in Fig. 1(d) and (e) describe the PC system, where τ_p is the disturbance torque from the P/S assemblies. Fig. 1(d) is commonly used to describe the closed-loop control of the pump discharge pressure p_d for a given reference f_r, whereas Fig. 1(e) focuses on analyzing the noise/disturbance effects on the control of the SP-angle β for a reference p_{di}.

As illustrated in Fig. 1(b) and (d), where the functional block "external loading mechanism" represents the dynamics from the SP-angle β to the resulting $p_{d\beta}$ in terms of a discharge flowrate as an intermediate variable not explicitly shown, the SP inclination (characterized by its primary angle β around the SP bearing axis) is adjusted by a mechanism where the pump discharge pressure p_d is fedback to the PC valve (sectional area A_v) and compared against the preload (or reference) force f_r of the valve spring (stiffness, k_v). The comparison error determines the valve displacement x_v to control the flowrate q_a and pressure p_a of the control actuator chamber. Combined with the torque from the SP bias-spring (preload force f_b and stiffness k_b), the pressure p_a acted on the sectional area A_a generates a torque τ_a to counteract the disturbance torque τ_p and adjust β to regulate the pump discharge flow and pressure p_d. The feedback pressure p_d and disturbance torque τ_p oscillate (period $2\pi/N$) around their respective steady-state values $(p_{d0},\ \tau_{p0})$ [10], [11], [13], [14], [21] due to the inherent pumping dynamics. Consequently, the SP-angle β also vibrates about its steady-state value β_0 as demonstrated numerically and/or experimentally in [15], [16], and [20]. Caused by the SP ripples β, an additional pulsating pressure component $p_{d\beta}$ (with a zero-average value) is superimposed on the inherent pressure component p_{di} (corresponding to β_0) to generate the feedback pressure p_d. In the following discussion, the variables $(\beta,\ p_d,\ \tau_p,\ p_a,\ x_v)$ represent the incremental changes from their respective steady-state values $(\beta_0,\ p_{d0},\ \tau_{p0},\ p_{a0},\ x_{v0})$ for the specified reference f_r. For completeness, the calculations of the relevant steady-state values are given in Appendix A.

Fig. 1(e) provides insights into the AHM (3) for analyzing a noisy PC system, where the SP oscillation β (or ripple) is the variable of interest while the pulsating variables $(p_d,\ \tau_p)$ are characterized by $(\mathbf{Y}_\ell,\ \mathbf{D}_\ell)$

$$\boldsymbol{\beta}_\ell = \mathbf{G}(\omega)\,\boldsymbol{\tau}_{p\ell} - \mathbf{H}(\omega)\,\mathbf{p}_{d\ell}. \tag{3}$$

By excluding the complex external loading mechanism dynamics from the forward path, β can be effectively characterized as a function of $(p_d,\ \tau_p)$ in terms of the speed-dependent transfer matrices $\mathbf{G}(\omega)$ and $\mathbf{H}(\omega)$ to be derived. The significance and formulation of (3) are detailed in the following sections; time-domain PC-PP dynamic model (see Section II-B) and derivation of the AHM (see Section II-C).

B. Time-Domain Dynamic Model for the PC-PP

The dynamics of the PC-PP system [see Fig. 1(a)] are contributed by two primary subsystems; swash-plate [see Fig. 1(c)], PC-valve controlled actuator [see Fig. 1(b)].

1) Swash-Plate Dynamics: Fig. 1(c) shows the coordinate systems and parameters, where the reference XYZ is at the SP pivot O (with X along its bearing axis and Z parallel to the pump shaft); and the moving xyz is attached to the SP (with z perpendicular to its surface). The coordinate transformation from XYZ to xyz is accomplished by two successive rotations, $\boldsymbol{\Gamma}_X(\beta)$ and $\boldsymbol{\Gamma}_y(\phi)$, in (4c), where the secondary SP-angle γ

(small fixed angle around the *Y*-axis) is often designed to reduce the discharge flow ripple and SP overall control effort [24], [25]

$$\mathbf{\Gamma}_X(\beta) = \begin{bmatrix} 1 & 0 & 0 \\ 0 & \cos\beta & \sin\beta \\ 0 & -\sin\beta & \cos\beta \end{bmatrix} \text{ and}$$

$$\mathbf{\Gamma}_y(-\phi) = \begin{bmatrix} \cos\phi & 0 & -\sin\phi \\ 0 & 1 & 0 \\ \sin\phi & 0 & \cos\phi \end{bmatrix} \tag{4a-b}$$

$$\tan\phi = \tan\gamma\cos\beta. \tag{4c}$$

The position coordinates $[x_n,\ y_n,\ a]^T$ of the nth P/S assembly ($n = 1, 2, \ldots, N$) are transformed to $\mathbf{r}_{pn}$ from xyz to XYZ by (5a) with (4a–c). In (5a), (r_p, θ_n) are the (distribution radius, angular position) of the nth P/S assembly from the X-axis [see Fig. 1(a)]; e is an offset between the Z-axis and pump shaft centerline; and a is an offset of the P/S ball-joint [see Fig. 1(c)] from the xy plane

$$\mathbf{r}_{pn} = \begin{bmatrix} r_p\cos\theta_n \\ r_p\sin\theta_n - e \\ Z_n \end{bmatrix} = \mathbf{\Gamma}_X^{-1}(\beta)\,\mathbf{\Gamma}_y^{-1}(-\phi) \begin{bmatrix} x_n \\ y_n \\ a \end{bmatrix} \tag{5a}$$

$$\text{where}\quad \theta_n = \theta_{10} + \omega_m t + 2\pi(n-1)/N \tag{5b}$$

$$Z_n = r_p(\sin\theta_n\tan\beta - \tan\gamma\cos\theta_n) - e\tan\beta + a/(\cos\phi\cos\beta). \tag{5c}$$

In (5a), the rotation matrices ($\mathbf{\Gamma}_X$ and $\mathbf{\Gamma}_y$) defined in (4a, b) are nonsingular since $\det[\mathbf{\Gamma}_X] = \det[\mathbf{\Gamma}_y] = 1$; thus, their inverse matrices exist. In (5b), θ_{10} is the initial position of first P/S assembly. Similarly, the local force vector $[0,\ 0,\ f_{zn}]^T$ of the nth P/S assembly is transformed to $\mathbf{f}_{pn}$ in the XYZ frame by (6a, b), where m_{ps} is the mass of the P/S assembly, and the pressure p_n of the nth piston chamber is enclosed by the cylindrical-bore and applied on the piston area A_p

$$\mathbf{f}_{pn} = \mathbf{\Gamma}_X^{-1}(\beta)\,\mathbf{\Gamma}_y^{-1}(-\phi) \begin{bmatrix} 0 \\ 0 \\ f_{zn} \end{bmatrix} = f_{Zn} \begin{bmatrix} \tan\gamma \\ -\tan\beta \\ 1 \end{bmatrix}. \tag{6a}$$

$$\text{where } f_{Zn} = p_n A_p - m_{ps}\ddot{Z}_n. \tag{6b}$$

When rotating, the nth piston chamber is alternatively connected with the low- and high-pressure kidney of the valve-plate [see Fig. 1(a)], where the transitions between high and low pressures are characterized by the angles $(\varphi_{rs},\ \varphi_{re})$ and $(\varphi_{fs},\ \varphi_{fe})$. The first subscript ($r$ or f) denotes the rise or fall of the pressure, while the second subscript (s or e) represents the start or end of the pressure transition. The pressure transients within the angles $(\varphi_{rs},\ \varphi_{re})$ and $(\varphi_{fs},\ \varphi_{fe})$ are related to the complex pumping dynamics and must be solved numerically [26].

Derived from the Newton second law, the SP dynamics (with moment of inertia I_s and viscous damping coefficient b_s) is given in (7a), where the pulsating torque τ_p from the N P/S assemblies [see Fig. 1(c)] is a function of β, and the PC control actuating τ_a [see Fig. 1(b)] depends on p_d

$$I_s\ddot{\beta} + b_s\dot{\beta} + k_b l_a^2\beta = \tau_p(\beta) - \tau_a(p_d) \tag{7a}$$

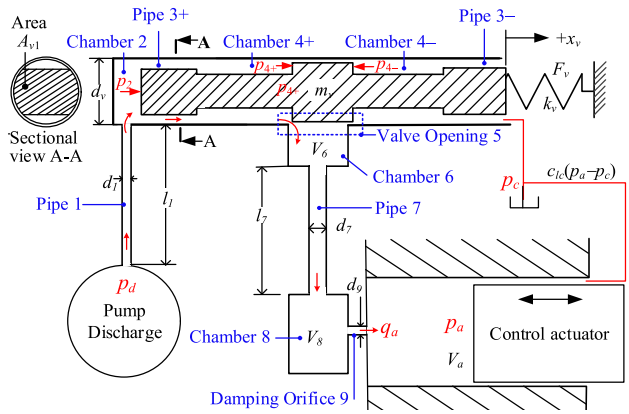

Fig. 2. Connecting hydraulic circuit that links the control actuator with the PC valve and feedback pressure.

$$\text{where } \tau_p = \sum_{n=1}^{N}\tau_{pn} = \sum_{n=1}^{N}[(\mathbf{r}_{pn}\times\mathbf{f}_{pn})\bullet\mathbf{u}_X] - \tau_{p0};$$

$$\tau_a = A_a l_a p_a. \tag{7b-c}$$

In (7b, c), l_a is an actuation arm [see Fig. 1(a)]; τ_{pn} is the X-component of the torque ripple acting on the SP calculated from $(\mathbf{r}_{pn}\times\mathbf{f}_{pn})\bullet\mathbf{u}_X$ (where $\mathbf{u}_X$ is the unit vector of the X-axis).

2) Control Actuator Dynamics: Different from τ_p that is directly related to β, the actuation torque τ_a or pressure p_a (7c) that counteracts the pulsating τ_p (7b) is implicitly related to the feedback pressure ripples p_d through the PC valve, control actuator, and connecting hydraulic (pipe/chamber) circuit as illustrated in Fig. 2. The PC valve that controls the flowrate q_v switches between positive and negative displacements to stroke or destroke the control actuator. For clarity, q_v through the PC valve at displacement x_v is formulated in terms of $q_{v\pm}$ and $x_{v\pm}$, where $(q_{v+},\ q_{v-})$ are defined as the flowrate through the PC valve when the displacement is (positive x_{v+}, negative x_{v-})

$$x_v = x_{v+} + x_{v-} = \begin{cases} x_{v+}, x_{v-} = 0 & x_v \geq 0 \\ x_{v-}, x_{v+} = 0 & x_v < 0 \end{cases} \tag{8a}$$

$$q_v = q_{v+}(x_{v+}) + q_{v-}(x_{v-}). \tag{8b}$$

In other words,

1) a positive flowrate q_a (from the discharge at p_d) that strokes the control actuator, flows through Pipe 1, Chamber 2, Pipe 3 + , Chamber 4 + , Valve opening 5 at x_{v+} Chamber 6, Pipe 7, Chamber 8 and Damping Pipe 9 into the actuator chamber V_a;
2) a negative rate q_a that destrokes the control flows through Pipe 9, Chamber 8, Pipe 7, Chamber 6, Valve opening 5 at x_{v-}, Chamber 4− and Pipe 3− and returns to the reservoir.

For ease of manufacturing, the valve-spool end-surfaces were flattened with Pipe 3± (same cross section but different aspect-ratio $\kappa = l_{3+}/l_3$) connecting Chamber 4± to (Chamber 2, pump reservoir) as shown in Fig. 2 (top-left), where A_{v1} and A_{v2} $(= A_v - A_{v1})$ are the effective cross-sectional areas. The dynamics of the PC valve displacement is governed by (9), where

$(m_v,\ b_v)$ are the (valve and 1/3 spring mass, viscous damping coefficient) respectively

$$m_v\ddot{x}_v + b_v\dot{x}_v + k_v x_v = p_2 A_{v1} + (p_{4+} - p_{4-})\, A_{v2}. \tag{9}$$

The dependence of p_a on q_a is defined by (10) considering the effect of fluid capacitance C_a, the flowrate $A_a l_a \dot{\beta}$ induced by the actuator movement and the leakage flow to the reservoir

$$C_a\dot{p}_a + c_{la}p_a = q_a + A_a l_a \dot{\beta}. \tag{10}$$

In (10),$C_a = (V_{a0} - A_a l_a \beta_0)/K_{\rm e}$, where V_{a0} is the actuator chamber volume at zero plate angle ($\beta_0 = 0$); K_e is the oil bulk modulus; and c_{la} is the actuator leakage coefficient.

The pressures (p_2 and $p_{4\pm}$) and flowrate q_a can be determined from the hydraulic circuit, where the flow dynamics of the pipes (length l_i and diameter d_i with $i = 1,\ 3\pm,\ 7,\ 9$) are modeled by their respective (inertance I_i, resistance R_i) in the following equation:

$$\frac{I_i}{R_i}\frac{dq_i}{dt} + q_i = \frac{1}{R_i}\begin{cases} p_{i-1} - p_{i+1} & i = 1, 7, 9 \\ p_2 - p_{4+} & i = 3+ \\ p_{4-} & i = 3- \end{cases} \tag{11}$$

where $\frac{I_i}{R_i} = \frac{d_i^2}{32\upsilon}$; $R_i = \frac{128\mu l_i}{\pi d_i^4}$; $p_0 = p_d$; $p_{10} = p_a$; and $(\upsilon,\ \mu)$ are the (kinematic, dynamic) viscosity of the hydraulic oil. Similarly, the fluid dynamics of the chambers (volume V_j where $j = 2, 4\pm, 6, 8$) characterized by their capacitance C_j are modeled in the following equation:

$$\frac{dp_j}{dt} = \begin{cases} (q_{j-1} - q_{j+1})/C_j & j = 2, 6, 8 \\ (\pm q_{3\pm} \mp q_{v\pm})/C_j & j = 4\pm \end{cases} \tag{12}$$

where $C_j = V_j/K_e$; $q_5 = q_v$ and $q_9 = q_a$. The flowrate $q_{v\pm}$ through the orifice (PC-valve opening) can be derived as follows:

$$\frac{q_{v\pm}}{x_{v\pm}} = \lambda_{\pm}\mathrm{sgn}\left(1 + \frac{\pm p_{4\pm} \mp p_6}{\pm p_{(4\pm)0} \mp p_{60}}\right)\sqrt{\left|1 + \frac{\pm p_{4\pm} \mp p_6}{\pm p_{(4\pm)0} \mp p_{60}}\right|} \tag{13a}$$

$$\text{and } \lambda_{\pm} = C_d w_{\pm}\sqrt{2\left(\pm p_{(4\pm)0} \mp p_{60}\right)/\rho}. \tag{13b}$$

In (13b) where C_d is the PC-valve discharge coefficient and $w_{\pm}$ are the circumferential opening lengths corresponding to $x_{v\pm}$, $(\pm p_{4\pm} \mp p_6)$ are normalized to their steady-state values $(\pm p_{(4\pm)0} \mp p_{60})$, where $p_{\ (4+)0} > p_{60} > p_{(4-)0}$ and hence $\lambda_{\pm} > 0$.

C. Derivation of Analytical Harmonic Model for a PC-PP

The PC-PP system [see Fig. 1(e)] governed by (9) to (12) is a 15th order system with nonlinear switching defined by (8a, b) and (13a), where the solutions require time-consuming numerical computations. As an alternative to investigate the (τ_p, p_d) effects on β under different operating speed ω_m, the AHM (3) that relates the SP-ripple $\boldsymbol{\beta}_\ell$ to $\boldsymbol{\tau}_{p\ell}(\beta_0)$ and $\mathbf{p}_{d\ell}$ is derived from the dynamic models of the SP and control actuator.

1) Swash-Plate Oscillations Linked to Disturbance: For a PC-PP ($m_{ps}, r_p, \gamma, a, e, A_p$) operated at a steady-state condition ($p_{d0},\ \omega_m,\ \beta_0$), the disturbance torque ripple τ_p (7b) depends on the nth piston pressure p_n (6b). With the pressure in the transitions [$(\varphi_{rs},\ \varphi_{re})$; $(\varphi_{fs},\ \varphi_{fe})$] approximated by a sinusoidal waveform [see Fig. 1(a)], p_n is formulated as a harmonic function of the angular position θ_n (period 2π) in (14a–c), where p_s is the pump suction pressure, $\hat{\varphi}_r = \varphi_{re} - \varphi_{rs}$and $\hat{\varphi}_f = \varphi_{fe} - \varphi_{fs}$

$$p_n = \sum_{k=1,2....}^{\infty} \mathbf{h}\,(k\theta_n)\,\mathbf{p}_{nk} \tag{14a}$$

$$\text{where } \frac{\mathbf{p}_{nk}}{p_{d0} - p_s} = \frac{\mathbf{T}_k}{2\pi k}\left[\frac{1}{1-(k/\pi)^2\hat{\varphi}_r^2}\ \ \frac{1}{1-(k/\pi)^2\hat{\varphi}_f^2}\right]^T \tag{14b}$$

$$\text{and } \mathbf{T}_k = \begin{bmatrix} \cos k\varphi_{rs} + \cos k\varphi_{re} & -\cos k\varphi_{fs} - \cos k\varphi_{fe} \\ -\sin k\varphi_{rs} - \sin k\varphi_{re} & \sin k\varphi_{fs} + \sin k\varphi_{fe} \end{bmatrix}. \tag{14c}$$

In (14c), $(\varphi_{rs}, \varphi_{re}, \varphi_{fs}, \varphi_{fe})$ can be determined from the p_n curve obtained numerically and experimentally. By substituting $\mathbf{r}_{pn}$ from (5a) and $\mathbf{f}_{pn}$ from (6a), where p_n is given by (14a) into (7b) and by using the orthogonality (1g), the disturbance dynamics (7b) is expressed explicitly in terms of $\boldsymbol{\tau}_{p\ell}$ and $\boldsymbol{\beta}_\ell$ to account for the steady-state variation $\tau_{p0}(\beta_0)$ caused by the SP oscillation

$$\tau_p\,(\beta) = \left.\frac{d\tau_{p0}\,(\beta)}{d\beta}\right|_{\beta=\beta_0}\sum_{\ell=1}^{\infty}\mathbf{h}\,(\ell N\theta)\,\boldsymbol{\beta}_\ell + \sum_{\ell=1}^{\infty}\left[\mathbf{h}\,(\ell N\theta_1)\,\boldsymbol{\tau}_{p\ell}\,(\beta_0)\right] - \left(I_{sa}\ddot{\beta} + c_{sa}\dot{\beta}^2 + b_{sa}\dot{\beta}\right). \tag{15}$$

The steady-state parameters in (15), τ_{p0}, $\boldsymbol{\tau}_{p\ell}$, the incremental moment of inertia I_{sa} and the (quadratic, viscous) damping coefficients (c_{sa}, b_{sa}) of the SP rotational system, are given in (A.2a–e). In (15), the $\boldsymbol{\tau}_{p\ell}$ term is measured from the first piston angular position θ_1, while the $\boldsymbol{\beta}_\ell$ term is formulated in terms of the operating position θ of the PP. The phase difference between the $\boldsymbol{\tau}_{p\ell}$ and $\boldsymbol{\beta}_\ell$ terms can be accounted for by a transformation matrix $\mathbf{T}_\ell(\ell N\alpha)$, where $\alpha = \theta - \theta_1$, with which (7a) is rewritten in harmonic form (16a) after substituting τ_p from (15), expressing p_a and β (and its time derivatives) in the form of (1a–c) and neglecting the quadratic terms of HAVs

$$\sum_{\ell=1...}^{\infty}\mathbf{h}\,(\ell N\theta)\left[\ell N\omega_m\bar{b}_s\mathbf{S}\boldsymbol{\beta}_\ell - (\ell N\omega_m)^2\bar{I}_s\mathbf{I}\,\boldsymbol{\beta}_\ell\right] = \sum_{\ell=1..}^{\infty}\mathbf{h}\,(\ell N\theta)\left[\mathbf{T}_\ell\boldsymbol{\tau}_{p\ell}\,(\beta_0) - \bar{k}_s\boldsymbol{\beta}_\ell - A_a l_a\mathbf{p}_{a\ell}\right] \tag{16a}$$

$$\text{where } \bar{I}_s = I_s + I_{sa}\,(\beta_0)\,;\bar{b}_s = b_s + b_{sa}\,(\beta_0) \tag{16b-c}$$

$$\bar{k}_s = k_b l_a^2 - \left.\frac{d\tau_{p0}}{d\beta}\right|_{\beta_0};\ \mathbf{T}_\ell(\ell N\alpha) = \begin{bmatrix} \cos(\ell N\alpha) & \sin(\ell N\alpha) \\ -\sin(\ell N\alpha) & \cos(\ell N\alpha) \end{bmatrix}. \tag{16d-e}$$

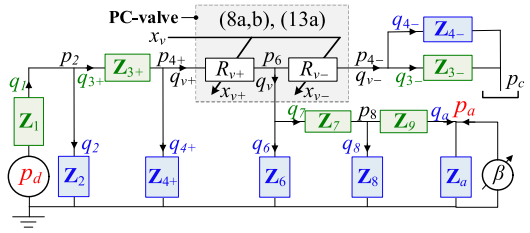

Fig. 3. Impedance representation of the hydraulic connecting circuit.

Expressed in terms of an impedance matrix $\mathbf{Z}_{s\ell}$ that describes the ℓth torque harmonics of the SP, (16a) is compactly written as follows:

$$\mathbf{Z}_{s\ell}(\omega)\,\boldsymbol{\beta}_\ell = \mathbf{T}_\ell \boldsymbol{\tau}_{p\ell}(\beta_0) - A_a l_a \mathbf{p}_{a\ell} \tag{17a}$$

$$\text{where } \mathbf{Z}_{s\ell}(\omega) = \bar{k}_s \mathbf{I} + (\ell\omega)\,\bar{b}_s \mathbf{S} - (\ell\omega)^2 \bar{I}_s \mathbf{I} \text{ and}$$

$$\omega = N\omega_m. \tag{17b-c}$$

2) Swash-Plate Oscillations Linked to PC-Feedback Noises: To derive the AHM (3) that relates $\boldsymbol{\beta}_\ell$ to $\mathbf{p}_{d\ell}$, the relationship between the HAV $\mathbf{p}_{a\ell}$ of the control-actuator pressure p_a (17a) and $\mathbf{p}_{d\ell}$ can be derived similarly from the dynamic model of the PC-valve controlled actuator, (8)–(13).

a) PC-valve displacement: For investigating the effects of the PC-valve displacement x_v on SP ripples, the valve flowrate (13a) is linearized and its HAV is formulated in (18a), where the positive steady-state value x_{v0} is given in (A.3f) and $\mathbf{x}_{(v\pm)\ell}$ are the HAVs of $x_{v\pm}$

$$\frac{\mathbf{q}_{(v\pm)\ell}}{\lambda_\pm} \approx \mathbf{x}_{(v\pm)\ell} \pm \frac{x_{v0}}{2}\frac{\pm\mathbf{p}_{(4\pm)\ell} \mp \mathbf{p}_{6\ell}}{\pm p_{(4\pm)0} \mp p_{60}}. \tag{18a}$$

From (8a), $\mathbf{x}_{v\ell} = \mathbf{x}_{(v+)\ell} + \mathbf{x}_{(v-)\ell}$ along with (18a), where $\lambda_\pm > 0$ as defined in (13b)

$$\mathbf{x}_{v\ell} = \frac{\mathbf{q}_{(v+)\ell}}{\lambda_+} + \frac{\mathbf{q}_{(v-)\ell}}{\lambda_-} + \frac{x_{v0}}{2}\left(\frac{\mathbf{p}_{6\ell} - \mathbf{p}_{(4-)\ell}}{p_{60} - p_{(4-)0}} - \frac{\mathbf{p}_{(4+)\ell} - \mathbf{p}_{6\ell}}{p_{(4+)0} - p_{60}}\right). \tag{18b}$$

From (9), the HAV $\mathbf{x}_{v\ell}$ corresponding to the PC-valve displacement x_v is derived in (19a), where $(\mathbf{p}_{2\ell}, \mathbf{p}_{4\ell\pm})$ are the respective HAVs of $(p_2, \mathrm{p}_{4\pm})$

$$\mathbf{Z}_{x\ell}\mathbf{x}_{v\ell} = A_{v1}\mathbf{p}_{2\ell} + A_{v2}\left[\mathbf{p}_{(4+)\ell} - \mathbf{p}_{(4-)\ell}\right] \tag{19a}$$

$$\text{where } \mathbf{Z}_{x\ell}(\omega) = k_v \mathbf{I} + (\ell\omega)\, b_v \mathbf{S} - (\ell\omega)^2 m_v \mathbf{I} \tag{19b}$$

b) Hydraulic circuit: To help visualize the interrelations among the hydraulic components modeled as impedances, Fig. 3 schematically shows an equivalent circuit of the PC-valve controlled actuator (see Fig. 2), where the flowrates satisfy the Kirchhof's current law: $q_1 = q_2 + q_{3+}$; $q_{3\pm} = \pm q_{v\pm} \pm q_{4\pm}$; $q_v = q_6 + q_7$; and $q_7 = q_8 + q_a$.

With Fig. 3, the impedance matrices $\mathbf{Z}_{i\ell}$ of the hydraulic pipes and chambers, (10)–(12), are formulated in (20a–c), where the admittance $\mathbf{Z}_{a\ell}^{-1}$in (20a) is written as a reciprocal of impedance to avoid introducing additional symbols

$$\mathbf{q}_{a\ell} + (\ell\omega)\, A_a l_a \mathbf{S}\boldsymbol{\beta}_\ell = \mathbf{Z}_{a\ell}^{-1}\mathbf{p}_{a\ell}$$

$$\text{where } \mathbf{Z}_{a\ell}^{-1} = c_{la}\mathbf{I} + (\ell\omega)\, C_a \mathbf{S} \tag{20a}$$

$$\mathbf{Z}_{i\ell}(\omega)\mathbf{q}_{i\ell} = \begin{cases} \mathbf{p}_{(i-1)\ell} - \mathbf{p}_{(i+1)\ell} & i = 1, 7, 9 \\ \mathbf{p}_{2\ell} - \mathbf{p}_{(4+)\ell} & i = 3+ \\ \mathbf{p}_{(4-)\ell} & i = 3- \end{cases}$$

$$\text{where } \mathbf{Z}_{i\ell}(\omega) = R_i\mathbf{I} + (\ell\omega)\, I_i \mathbf{S} \tag{20b}$$

$$\mathbf{p}_{j\ell} = \mathbf{Z}_{j\ell}(\omega)\mathbf{q}_{j\ell} = \begin{cases} \mathbf{Z}_{j\ell}(\omega)\left[\mathbf{q}_{(j-1)\ell} - \mathbf{q}_{(j+1)\ell}\right] & j = 2, 6, 8 \\ \mathbf{Z}_{j\ell}(\omega)\left[\pm\mathbf{q}_{(3\pm)\ell} \mp \mathbf{q}_{(v\pm)\ell}\right] & j = 4\pm \end{cases}$$

$$\text{where } \mathbf{Z}_{j\ell}(\omega) = -(\ell\omega C_j)^{-1}\mathbf{S}. \tag{20c}$$

Unlike the $(\boldsymbol{\beta}_\ell,\ \boldsymbol{\tau}_{p\ell})$ relationship characterized by a single mechanical impedance (17b), $\mathbf{p}_{d\ell}$ and $\mathbf{p}_{a\ell}$ are implicitly related by the HAVs ($\mathbf{p}_{(4+)\ell}$, $\mathbf{p}_{6\ell}$ and $\mathbf{q}_{(v+)\ell}$) in the PC-valve (18a,b) and (19a,b). These implicit relations are derived from (20a–c), which are the defined impedances and the continuity equations at the nodal pressures (p_2, p_{4+}, p_8, and p_{4-}).

1) From $\mathbf{q}_{1\ell} = \mathbf{q}_{2\ell} + \mathbf{q}_{(3+)\ell}$ with the flowrates defined in (20b) with $i = 1$ and (20c) with $j = 2$ and 4 +

$$\mathbf{p}_{d\ell} = \boldsymbol{\rho}_{12}\mathbf{p}_{2\ell} + \boldsymbol{\rho}_{14}\mathbf{p}_{(4+)\ell} + \mathbf{Z}_{1\ell}\mathbf{q}_{(v+)\ell}$$

$$\text{where } \boldsymbol{\rho}_{12} = \mathbf{I} + \mathbf{Z}_{1\ell}\mathbf{Z}_{2\ell}^{-1} \text{ and } \boldsymbol{\rho}_{14} = \mathbf{Z}_{1\ell}\mathbf{Z}_{(4+)\ell}^{-1}. \tag{21a}$$

2) From $\mathbf{q}_{(3+)\ell} = \mathbf{q}_{(v+)\ell} + \mathbf{q}_{(4+)\ell}$ with the flowrates expressed in terms of pressures using (20b) with $i = 3+$ and (20c) with $j = 4+$

$$\mathbf{p}_{2\ell} = \boldsymbol{\rho}_{34}\mathbf{p}_{(4+)\ell} + \mathbf{Z}_{(3+)\ell}\mathbf{q}_{(v+)l}$$

$$\text{where } \boldsymbol{\rho}_{34} = \mathbf{I} + \mathbf{Z}_{(3+)\ell}\mathbf{Z}_{(4+)\ell}^{-1}. \tag{21b}$$

3) From $\mathbf{q}_{7\ell} = \mathbf{q}_{8\ell} + \mathbf{q}_{a\ell}$ with the flowrates given by (20b) with $i = 7$ and 9 and (20c) with $j = 8$

$$\mathbf{p}_{6\ell} = \boldsymbol{\rho}_{78}\mathbf{p}_{a\ell} + \mathbf{Z}_{\mathrm{T}\ell}\mathbf{q}_{a\ell}$$

$$\text{where } \boldsymbol{\rho}_{78} = \left(\mathbf{I} + \mathbf{Z}_{7\ell}\mathbf{Z}_{8\ell}^{-1}\right) \text{ and } \mathbf{Z}_{\mathrm{T}\ell} = \mathbf{Z}_{9\ell} + \mathbf{Z}_{7\ell}\mathbf{Z}_{8\ell}^{-1}\mathbf{Z}_{9\ell} + \mathbf{Z}_{7\ell}. \tag{21c}$$

4) The flowrate $\mathbf{q}_{v\ell} = \mathbf{q}_{(v+)\ell} + \mathbf{q}_{(v-)\ell}$ can be expressed in terms of ($\mathbf{p}_{6\ell}$, $\mathbf{p}_{a\ell}$, $\mathbf{q}_{a\ell}$) using (20b) with $i = (7, 9)$ and (20c) with $j = 8$

$$\mathbf{q}_{v\ell} = \mathbf{Z}_{6\ell}^{-1}\mathbf{p}_{6\ell} + \mathbf{Z}_{8\ell}^{-1}\mathbf{p}_{a\ell} + \boldsymbol{\rho}_{89}\mathbf{q}_{a\ell}$$

$$\text{where } \boldsymbol{\rho}_{89} = \mathbf{I} + \mathbf{Z}_{8\ell}^{-1}\mathbf{Z}_{9\ell}. \tag{21d}$$

5) From Fig. 3, we have (21e) where the minus sign before $\mathbf{q}_{(v-)\ell}$ is used to negate flowrate q_v- defined in (13a)

$$-\mathbf{q}_{(v-)\ell} = \mathbf{Z}_{p\ell}^{-1}\mathbf{p}_{(4-)\ell} \text{ where } \mathbf{Z}_{p\ell}^{-1} = \mathbf{Z}_{(4-)\ell}^{-1} + \mathbf{Z}_{(3-)\ell}^{-1}. \tag{21e}$$

The admittances $\mathbf{Z}_{j\ell}^{-1} = -\ell\omega C_j \mathbf{S}^{-1}$ wherein (21a–e), which are written as a reciprocal of the impedance defined in (20c), are nonsingular since $\det[\mathbf{S}] = 1$, where $\mathbf{S}$ is defined in (1f). Similarly, the inverse matrix of a pipe, for example, $\mathbf{Z}_{(3-)\ell}^{-1}$ in (21e) exists because of nonzero flow resistance in real pipes. The same argument can be made for the existence of the admittance $\mathbf{Z}_{p\ell}^{-1}$ for the network composed of chamber $\mathbf{Z}_{4-}$ and pipe $\mathbf{Z}_{3-}$ in parallel as shown in Figs. 2 and 3.

3) Procedure for Deriving the PC-PP AHM: To derive the AHM (3) that directly relates $\boldsymbol{\beta}_\ell$ to $\mathbf{p}_{d\ell}$ and $\boldsymbol{\tau}_{p\ell}$, the intermediate HAVs variables [$(\mathbf{p}_{a\ell}, \mathbf{q}_{a\ell})$, $(\mathbf{p}_{2\ell}, \mathbf{x}_{v\ell})$ and $\mathbf{p}_{(4\pm)\ell}$] are eliminated from the hydraulic circuit equations so that the remaining two variables ($\mathbf{p}_{6\ell}$, $\mathbf{q}_{v\ell}$) are only functions of $\mathbf{p}_{d\ell}$ and $\boldsymbol{\tau}_{p\ell}$. The procedure involves the following steps.

Step 1: Eliminate ($\mathbf{p}_{a\ell}$, $\mathbf{q}_{a\ell}$) from ($\mathbf{p}_{6\ell}$, $\mathbf{q}_{v\ell}$) by substituting (17a) and (20a) into (21c) and (21d)

$$(A_a l_a)\,\mathbf{p}_{6\ell} = \boldsymbol{\rho}_{\mathbf{h}}\mathbf{T}_\ell\boldsymbol{\tau}_{p\ell} - \mathbf{Z}_{\mathbf{m}}\boldsymbol{\beta}_\ell$$

$$\text{where } \mathbf{Z}_{\mathbf{m}} = \boldsymbol{\rho}_h\mathbf{Z}_{s\ell} + \ell\omega A_a^2 l_a^2 \mathbf{Z}_{\mathrm{T}\ell}\mathbf{S}$$

$$\text{and } \boldsymbol{\rho}_h = \boldsymbol{\rho}_{78} + \mathbf{Z}_{\mathrm{T}\ell}\mathbf{Z}_{a\ell}^{-1} \tag{22a}$$

$$(A_a l_a)\,\mathbf{q}_{v\ell} = \mathbf{Z}_{\mathbf{h}}^{-\mathbf{1}}\mathbf{T}_\ell\boldsymbol{\tau}_{p\ell} - \boldsymbol{\rho}_{\mathbf{hm}}\boldsymbol{\beta}_\ell$$

$$\text{where } \mathbf{Z}_{\mathbf{h}}^{-\mathbf{1}} = \mathbf{Z}_{6\ell}^{-1}\boldsymbol{\rho}_{\mathbf{h}} + \mathbf{Z}_{8\ell}^{-1} + \boldsymbol{\rho}_{89}\mathbf{Z}_{a\ell}^{-1};$$

$$\text{and } \boldsymbol{\rho}_{\mathbf{hm}} = \mathbf{Z}_{\mathbf{h}}^{-\mathbf{1}}\mathbf{Z}_{s\ell} + \ell\omega A_a^2 l_a^2\left(\boldsymbol{\rho}_{89} + \mathbf{Z}_{6\ell}^{-1}\mathbf{Z}_{\mathrm{T}\ell}\right)\mathbf{S}. \tag{22b}$$

In (22a, b), ($\mathbf{p}_{6\ell}$, $\mathbf{q}_{v\ell}$) are derived as a function of $\boldsymbol{\beta}_\ell$ and $\boldsymbol{\tau}_{p\ell}$; and $\mathbf{Z}_{\mathbf{h}}^{-1}$ is the admittance of the network formed by the chambers ($\mathbf{Z}_6$, $\mathbf{Z}_8$) and the pipe ($\mathbf{Z}_7$, $\mathbf{Z}_9$) as shown in Figs. 2 and 3.

Step 2: Eliminate $\mathbf{p}_{2\ell}$ (that relates $\mathbf{x}_{v\ell}$ and $\mathbf{p}_{d\ell}$), $\mathbf{x}_{v\ell}$ and $\mathbf{p}_{(4\pm)\ell}$. Given that the pressure ($p_{4\pm}$) effect on the valve displacement can be accounted for in (19a), the pressure across the valve opening is neglected (or $\mathbf{p}_{6\ell} = \mathbf{p}_{(4+)\ell}$) in computing $\mathbf{q}_{v\ell}$ (18b); in other words, $\mathbf{q}_{v\ell}$ is controlled by the valve displacement $\mathbf{x}_{v\ell}$. To begin with, substitute $\mathbf{p}_{2\ell}$ (21b) and (21e) into (19a) leading to (23a), where $\rho_A = A_{v2}/A_{v1}$ and $A_{v1} \neq 0$

$$A_{v1}^{-1}\mathbf{Z}_{x\ell}\mathbf{x}_{v\ell} = (\boldsymbol{\rho}_{34} + \rho_A\mathbf{I})\,\mathbf{p}_{6\ell} + \mathbf{Z}_{(3+)\ell}\mathbf{q}_{v\ell} + \left(\mathbf{Z}_{(3+)\ell}\mathbf{Z}_{p\ell}^{-1} - \rho_A\mathbf{I}\right)\mathbf{p}_{(4-)\ell}. \tag{23a}$$

Then, eliminate $\mathbf{x}_{v\ell}$ from the above using (18b) resulting in

$$\boldsymbol{\rho}_{4+}\mathbf{p}_{6\ell} = \left(A_{v1}^{-1}\lambda_+^{-1}\mathbf{Z}_{x\ell} - \mathbf{Z}_{3\ell+}\right)\mathbf{q}_{v\ell} + \boldsymbol{\rho}_{4-}\mathbf{p}_{(4-)\ell}$$

$$\text{where } \boldsymbol{\rho}_{4+} = (\boldsymbol{\rho}_{34} + \rho_A\mathbf{I}) - C_o\mathbf{Z}_{x\ell};$$

$$C_o = \frac{x_{v0}}{2A_{v1}\left(p_{60} - p_{(4-)0}\right)};$$

$$\text{and } \boldsymbol{\rho}_{4-} = A_{v1}^{-1}\left(\lambda_+^{-1} - \lambda_-^{-1}\right)\mathbf{Z}_{x\ell}\mathbf{Z}_{p\ell}^{-1} - \left(\mathbf{Z}_{3\ell+}\mathbf{Z}_{p\ell}^{-1} - \rho_A\mathbf{I}\right) - C_o\mathbf{Z}_{x\ell}. \tag{23b}$$

Next, substitute (21b, e) into (21a) leading to (23c)

$$\mathbf{p}_{d\ell} = (\boldsymbol{\rho}_{12}\boldsymbol{\rho}_{34} + \boldsymbol{\rho}_{14})\,\mathbf{p}_{6\ell} + \left(\boldsymbol{\rho}_{12}\mathbf{Z}_{(3+)\ell} + \mathbf{Z}_{1\ell}\right)\left(\mathbf{q}_{v\ell} + \mathbf{Z}_{p\ell}^{-1}\mathbf{p}_{(4-)\ell}\right). \tag{23c}$$

After eliminating $\mathbf{p}_{(4-)\ell}$ from the above pair of (23b, c), we have (23d) relating ($\mathbf{p}_{6\ell}$, $\mathbf{q}_{v\ell}$) to $\mathbf{p}_{d\ell}$

$$\boldsymbol{\rho}_{\mathbf{d}}\mathbf{p}_{d\ell} = \mathbf{Z}_{\mathbf{v}}\mathbf{q}_{v\ell} + \boldsymbol{\rho}_{\mathbf{v}}\mathbf{p}_{6\ell}$$

$$\text{where } \boldsymbol{\rho}_{\mathbf{d}} = \boldsymbol{\rho}_{4-}\left[\left(\boldsymbol{\rho}_{12}\mathbf{Z}_{(3+)\ell} + \mathbf{Z}_{1\ell}\right)\mathbf{Z}_{p\ell}^{-1}\right]^{-1};$$

$$\boldsymbol{\rho}_{\mathbf{v}} = \boldsymbol{\rho}_{\mathbf{d}}\left(\boldsymbol{\rho}_{12}\boldsymbol{\rho}_{34} + \boldsymbol{\rho}_{14}\right) + \boldsymbol{\rho}_{4+}$$

$$\text{and } \mathbf{Z}_{\mathbf{v}} = \boldsymbol{\rho}_{4-}\mathbf{Z}_{p\ell} + \mathbf{Z}_{(3+)\ell} - A_{v1}^{-1}\lambda_+^{-1}\mathbf{Z}_{x\ell}. \tag{23d}$$

Step 3: Derive ($\mathbf{G}$, $\mathbf{H}$) in (3) which account for all the elements from the pump discharge port to the SP. By substituting ($\mathbf{p}_{6\ell}$, $\mathbf{q}_{v\ell}$) from (22a, b) into (23d)

$$(\mathbf{Z}_{\mathbf{v}}\boldsymbol{\rho}_{\mathbf{hm}} + \boldsymbol{\rho}_{\mathbf{v}}\mathbf{Z}_{\mathbf{m}})\,\boldsymbol{\beta}_\ell = \left(\mathbf{Z}_{\mathbf{v}}\mathbf{Z}_{\mathbf{h}}^{-\mathbf{1}} + \boldsymbol{\rho}_{\mathbf{v}}\boldsymbol{\rho}_{\mathbf{h}}\right)\mathbf{T}_\ell\boldsymbol{\tau}_{p\ell} - (A_a l_a\boldsymbol{\rho}_{\mathrm{d}})\,\mathbf{p}_{d\ell}. \tag{24}$$

Rewriting (24) in the form suggested by (3), ($\mathbf{G}$, $\mathbf{H}$) are deduced in (25a, b) with $\mathbf{T}_\ell$ defined in (16e), the equivalent impedances in (26a–e) and the pressure ratios in (27a–e)

$$\mathbf{G}(\omega) = \left(\mathbf{Z}_{\mathbf{v}}\boldsymbol{\rho}_{\mathbf{hm}} + \boldsymbol{\rho}_{\mathbf{v}}\mathbf{Z}_{\mathbf{m}}\right)^{-1}\left(\mathbf{Z}_{\mathbf{v}}\mathbf{Z}_{\mathbf{h}}^{-\mathbf{1}} + \boldsymbol{\rho}_{\mathbf{v}}\boldsymbol{\rho}_{\mathbf{h}}\right)\mathbf{T}_\ell \tag{25a}$$

$$\mathbf{H}(\omega) = A_a l_a\left(\mathbf{Z}_{\mathbf{v}}\boldsymbol{\rho}_{\mathbf{hm}} + \boldsymbol{\rho}_{\mathbf{v}}\mathbf{Z}_{\mathbf{m}}\right)^{-1}\boldsymbol{\rho}_{\mathrm{d}} \tag{25b}$$

$$\mathbf{Z}_{\mathbf{m}}(\omega) = \boldsymbol{\rho}_{\mathbf{h}}\left[-(\ell\omega)^2\bar{I}_{\mathrm{s}}\mathbf{I} + (\ell\omega)\,\bar{b}_s\mathbf{S} + \bar{k}_s\mathbf{I}\right] + \ell\omega(A_a l_a)^2\mathbf{Z}_{\mathrm{T}\ell}\mathbf{S}; \tag{26a}$$

$$\mathbf{Z}_{\mathbf{v}}(\omega) = -A_{v1}^{-1}\lambda_+^{-1}\left[-(\ell\omega)^2 m_v\mathbf{I} + k_v\mathbf{I} + \ell\omega b_v\mathbf{S}\right] + \boldsymbol{\rho}_{4-}\mathbf{Z}_{p\ell} + \mathbf{Z}_{(3+)\ell}; \tag{26b}$$

$$\text{and } \mathbf{Z}_{\mathbf{h}}^{-\mathbf{1}} = \mathbf{Z}_{6\ell}^{-1}\boldsymbol{\rho}_h + \mathbf{Z}_{8\ell}^{-1} + \boldsymbol{\rho}_{89}\mathbf{Z}_{a\ell}^{-1}; \tag{26c}$$

$$\text{where } \mathbf{Z}_{\mathrm{T}\ell} = \mathbf{Z}_{9\ell} + \mathbf{Z}_{7\ell}\mathbf{Z}_{8\ell}^{-1}\mathbf{Z}_{9\ell} + \mathbf{Z}_{7\ell}; \tag{26d}$$

$$\mathbf{Z}_{p\ell}^{-1} = \mathbf{Z}_{(4-)\ell}^{-1} + \mathbf{Z}_{(3-)\ell}^{-1} \text{ and } \omega = N\omega_m \tag{26e-f}$$

$$\boldsymbol{\rho}_{\mathrm{d}} = \left[\begin{array}{l} A_{v1}^{-1}\left(\lambda_+^{-1} - \lambda_-^{-1}\right)\mathbf{Z}_{x\ell}\mathbf{Z}_{p\ell}^{-1} - \\ \left(\rho_A\mathbf{I} - \mathbf{Z}_{3\ell+}\mathbf{Z}_{p\ell}^{-1}\right) - C_o\mathbf{Z}_{x\ell} \end{array}\right] \times \left[\left(\boldsymbol{\rho}_{12}\mathbf{Z}_{(3+)\ell} + \mathbf{Z}_{1\ell}\right)\mathbf{Z}_{p\ell}^{-1}\right]^{-1} \tag{27a}$$

$$\boldsymbol{\rho}_{\mathbf{h}} = \boldsymbol{\rho}_{78} + \mathbf{Z}_{\mathrm{T}\ell}\mathbf{Z}_{a\ell}^{-1} \tag{27b}$$

$$\boldsymbol{\rho}_{\mathbf{hm}} = \mathbf{Z}_{\mathbf{h}}^{-\mathbf{1}}\mathbf{Z}_{s\ell} + \ell\omega(A_a l_a)^2\left(\boldsymbol{\rho}_{89} + \mathbf{Z}_{6\ell}^{-1}\mathbf{Z}_{\mathrm{T}\ell}\right)\mathbf{S} \tag{27c}$$

$$\boldsymbol{\rho}_{\mathbf{v}} = \boldsymbol{\rho}_{\mathrm{d}}\left(\boldsymbol{\rho}_{12}\boldsymbol{\rho}_{34} + \boldsymbol{\rho}_{14}\right) + (\boldsymbol{\rho}_{34} + \rho_A\mathbf{I}) - C_o\mathbf{Z}_{x\ell} \tag{27d}$$

$$\text{and } \boldsymbol{\rho}_{ij} = \mathbf{I} + \mathbf{Z}_{i\ell}^{-1}\mathbf{Z}_{j\ell}; \tag{27e}$$

$$\text{where } \rho_A = \frac{A_{v2}}{A_{v1}} \text{ and } C_o = \frac{x_{v0}}{2A_{v1}\left(p_{60} - p_{(4-)0}\right)}. \tag{27f-g}$$

The parameters (inertia, damping coefficient, and stiffness) in (26a, b) of $\mathbf{Z}_{\mathbf{m}}$ and $\mathbf{Z}_{\mathbf{v}}$ are defined in (16b–c) and (19b). For a stable-controlled system, it is always possible to derive nonsingular transfer functions, $\mathbf{G}(\omega)$ and $\mathbf{H}(\omega)$ as defined in (25a, b) describing the dynamics of periodic torque disturbance and feedback noises on the manipulated variables, respectively. In general, the poles that can be derived from the characteristic equation $\det[\mathbf{Z}_{\mathbf{v}}\boldsymbol{\rho}_{\mathbf{hm}} + \boldsymbol{\rho}_{\mathbf{v}}\mathbf{Z}_{\mathbf{m}}] = 0$ are on the left-half complex plane for the stable-controlled system, which account for the coupling between the mechanical and hydraulic subsystems.

4) Computing Steps for Analyzing Swash-Plate Oscillation: The transfer matrices ($\mathbf{G}$, $\mathbf{H}$) derived in (25a, b) provide a basis to

TABLE I
NOMENCLATURE AND PARAMETRIC VALUES OF THE PC-PP

Items	Parameter	Unit	Value
Piston Pump			
Case pressure	p_c	MPa	0.5
Piston number	N		9
Piston pitch radius	r_p	mm	13.6
Piston cross-sectional area	A_p	mm^2	46.1
Mass of P/S assembly	m_{ps}	g	9.3
Offsets	(a, e)	mm	(1.7, −2)
Oil bulk modulus	K_e,	MPa	1100
Operating speed	n_r	rpm	2400~4200
Secondary swash-plate angle	γ	°	−3
Swash-Plate Control Mechanism			
Control actuator area	A_a	m^2	50.15
Moment of inertia	I_s	kg.mm^2	40.57
Actuation force arm	l_a	mm	21.15
Spring preload and stifness	(f_b, k_b)	N, N/m	(8, 22000)
PC Valve			
Spring preload and stiffness	(f_r, k_v)	N, N/m	(90, 48000)
Cross-sectional areas	(A_{v1}, A_{v2})	mm^2	(4.16, 0.36)
Mass and damping coefficient	m_v, b_v	g, Ns/m	(1.93, 0.1)
Hydraulic Circuit			
Pipe 1 (length, diameter)	l_1, d_1	mm	(38, 2)
Chambers (2, 4±) volume	V_2, $V_{4\pm}$	mm^3	(122.7, 3.56)
Pipe 3± (length, diameter)	$l_{3\pm}$, d_3	mm	(8, 5), 0.68
Chambers (6, 8) Volume	V_6, V_8	mm^3	(31.7, 1414)
Pipe 7 (length, diameter)	l_7, d_7	mm	(30, 2)
Pipe 9 (length. Diameter)	l_9, d_9	mm	(2, 2)

analyze the SP oscillation from measured HF discharge pressure p_d, where the computation involves the following three stages.

1) For a given piston pump with known geometric/operating parameters $(p_{d0}, \beta_0, \omega_m)$, determine the steady-state values $(\tau_{p0}, p_{a0}, q_{a0}, p_{60}, p_{(4\pm)0}, x_{v0}, p_{20})$ according to Appendix A.
2) Formulate (**G**, **H**) according to (25a, b), along with the equivalent impedances (26a–e), pressure ratios (27a–g), and hydraulic impedances (see Figs. 2 and 3) defined in (20a–c).
3) Compute $\boldsymbol{\beta}_\ell$ (and hence β of the SP) from (3) with $\boldsymbol{\tau}_{p\ell}$ derived in (A.2b) and $\mathbf{p}_{d\ell}$ determined from the measured discharge pressure p_d. With calculated $\boldsymbol{\beta}_\ell$, the (amplitude, phase) of the ℓth harmonic of β can be obtained in the form of (1a, d, e). Note that the angle α in $\mathbf{T}_\ell(\alpha)$ can be identified from the comparison between the measured and computed β at the initial stage of the pump operations. Once determined, α keeps constant during every operations of the pump.

III. RESULTS AND DISCUSSIONS

An investigation was conducted on an aircraft PC-PP (see Fig. 1) to illustrate and validate the AHM, and analyze the HF oscillation characteristics of the SP under various operating speeds. The parametric values of the PC-PP used in the investigation are listed in Table I. Fig. 4 illustrates the test rig and setup used in the experiments, where the pump was driven by a variable-frequency electric motor; and an adjustable throttle valve was connected to its discharge port as a load as shown in Fig. 4(a). An HF pressure sensor was installed to measure the discharge pressure p_d. The SP-angle β was measured by a high-precision potentiometric angle sensor (P6500 series @

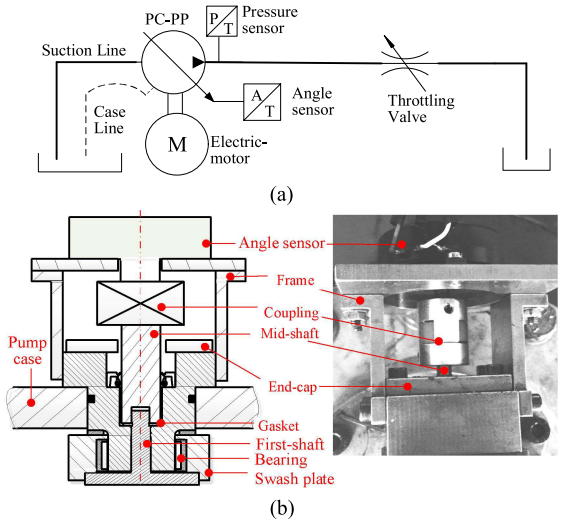

Fig. 4. Test rig. (a) Schematic diagram. (b) Swash-plate angle measurement device installed on the aircraft pump case.

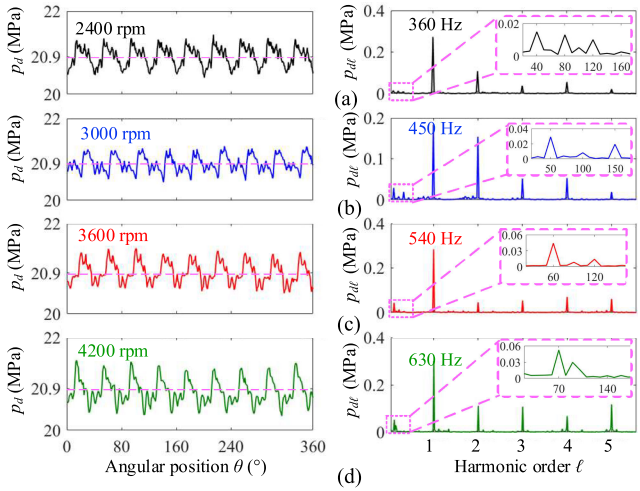

Fig. 5. Discharge pressure. (a) 2400 r/min. (b) 3000 r/min. (c) 3600 r/min. (d) 4200 r/min. Left: Time domain. Right: Frequency domain.

Novotechnik) mounted on the pump case through a frame [see Fig. 4(b)]; and the SP rotation was transmitted to its input shaft via the mid-shaft/ coupling.

Due to stringent lubrication conditions of the friction pairs, mechanical dynamics, and oil cavitation, hydraulic piston pumps are often operated within an upper limit beyond which the sharply increased wear and vibrations of the overall pump will greatly influence the swash-plate angle measurements. Equations (25)–(27) reveal that β_0 has little effect on $\mathbf{G}(\omega)$ and $\mathbf{H}(\omega)$ and hence the swash-plate HF oscillation characteristics, which is consistent with that reported in [15] and [21]. Thus, the following discussions are based on four typical pump speeds $n_r = 60\omega_m/2\pi$ (= 2400, 3000, 3600, 4200) r/min operated at the same steady-state discharge pressure p_{d0} at 20.9MPa, while the SP was kept at the mid-position ($\beta_0 = 8°$–$10°$). During experiments, p_d and β were simultaneously sampled at a rate of 20 kHz. The results are summarized in Figs. 5 –7, and Tables II

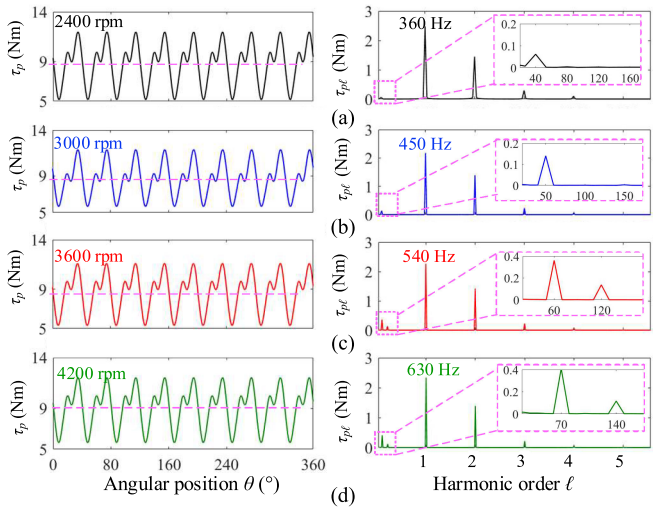

Fig. 6. Disturbance torque. (a) 2400 r/min. (b) 3000 r/min. (c) 3600 r/min. (d) 4200 r/min. Left: Time domain. Right: Frequency domain.

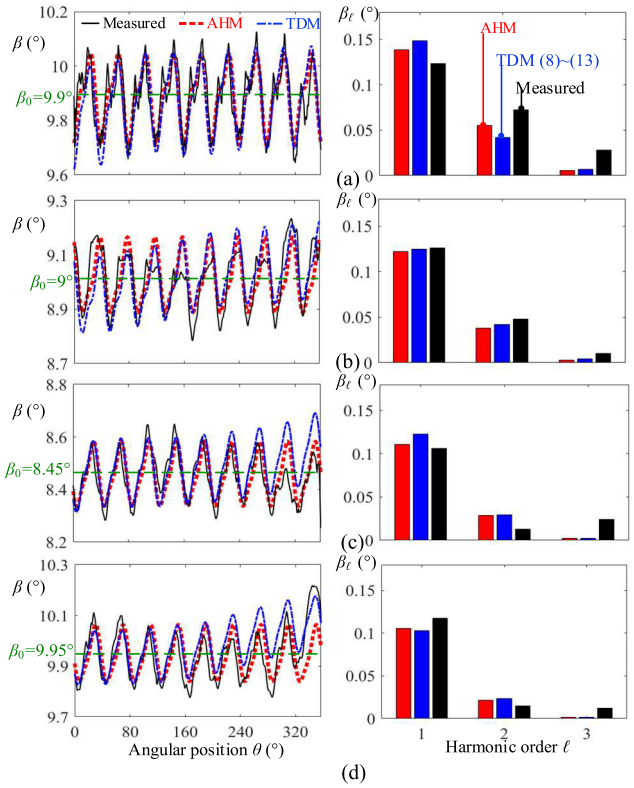

Fig. 7. Swash-plate HF oscillations; Comparisons between proposed AHM and conventional TDM. (a) 2400 r/min. (b) 3000 r/min. (c) 3600 r/min. (d) 4200 r/min. Left: Time domain. Right: Frequency domain.

and III. To validate the AHM and demonstrate its potential advantages for real-time applications, the β calculated by the AHM (see Section II-C) and the conventional TDM described in Section II-B and their required computation times (based on laptop with 2.3 GHz CPU and 16G memory) are compared with that measured experimentally in Fig. 7 and in Table III (last row), respectively.

TABLE II
HAVs OF THE DISCHARGE PRESSURE AND DISTURBANCE TORQUE

ℓ=1,2,3	n_r=2400 rpm	3000 rpm	3600 rpm	4200 rpm
$\boldsymbol{\tau}_{p\ell}$ Nm 1	$[-2.450\ 0.056]^T$	$[-2.08\ 0.55]^T$	$[-2.28\ -0.032]^T$	$[-2.31\ -0.076]^T$
$\boldsymbol{\tau}_{p\ell}$ Nm 2	$[-1.190\ 0.850]^T$	$[-1.14\ 0.79]^T$	$[-1.15\ 0.77]^T$	$[-1.18\ 0.77]^T$
$\boldsymbol{\tau}_{p\ell}$ Nm 3	$[0.007\ -0.290]^T$	$[0.01\ -0.23]^T$	$[-0.013\ -0.21]^T$	$[-0.004\ -0.22]^T$
$\mathbf{p}_{d\ell}$ MPa 1	$[-0.272\ 0.023]^T$	$[0.014\ 0.182]^T$	$[-0.25\ 0.13]^T$	$[-0.26\ -0.17]^T$
$\mathbf{p}_{d\ell}$ MPa 2	$[-0.065\ 0.089]^T$	$[-0.15\ -0.034]^T$	$[0.011\ -0.044]^T$	$[0.045\ 0.093]^T$
$\mathbf{p}_{d\ell}$ MPa 3	$[0.012\ -0.038]^T$	$[0.047\ 0.024]^T$	$[-0.053\ -0.008]^T$	$[0.11\ -0.021]^T$
τ_{p0} (Nm)	8.76	8.71	8.7	9.1
β_0 (°)	9.9	9	8.45	9.95

TABLE III
HAV OF THE SWASH-PLATE ANGLE AND COMPUTATION TIME

n_r	ℓ	$\mathbf{G}(\omega)\,\mathbf{p}_{d\ell}$	$\mathbf{H}(\omega)\,\boldsymbol{\tau}_{p\ell}$	$\boldsymbol{\beta}_\ell$
2400 rpm	1	$-[0.0044\ \ 0.145]^T$	$[8.6\ \ -7]^T\times10^{-3}$	$-[0.013\ \ 0.138]^T$
	2	$[0.046\ \ -0.31]^T$	$-[4.9\ \ 8.3]^T\times10^{-4}$	$[0.046\ \ -0.03]^T$
	3	$-[4.5\ \ 4]^T\times10^{-3}$	$[2.6\ \ -1.4]^T\times10^{-5}$	$-[4.6\ \ 3.7]^T\times10^{-3}$
3000 rpm	1	$[-0.077\ \ 0.096]^T$	$-[4\ \ 3]^T\times10^{-3}$	$[-0.073\ \ 0.099]^T$
	2	$[-0.009\ \ 0.037]^T$	$-[1.3\ \ 0.88]^T\times10^{-5}$	$[-0.009\ \ 0.037]^T$
	3	$-[1.3\ \ 3]^T\times10^{-3}$	$[1\ \ 2]^T\times10^{-5}$	$-[1.3\ \ 2.9]^T\times10^{-3}$
3600 rpm	1	$-[0.104\ \ 0.043]^T$	$-[0.067\ \ 4]^T\times10^{-3}$	$-[0.104\ \ 0.039]^T$
	2	$-[0.015\ \ 0.024]^T$	$[1.6\ \ -1.25]^T\times10^{-5}$	$-[0.015\ \ 0.024]^T$
	3	$[0.077\ \ 2]^T\times10^{-3}$	$-[7.3\ \ 6.2]^T\times10^{-6}$	$[0.08\ \ 2.2]^T\times10^{-3}$
4200 rpm	1	$-[0.101\ \ 0.019]^T$	$[3\ \ -2]^T\times10^{-3}$	$-[0.104\ \ 0.017]^T$
	2	$-[0.014\ \ 0.017]^T$	$[-0.5\ \ 3.6]^T\times10^{-5}$	$-[0.014\ \ 0.017]^T$
	3	$[0.13\ \ 2]^T\times10^{-3}$	$[10\ \ 7.7]^T\times10^{-6}$	$[0.12\ \ 1.6]^T\times10^{-3}$
Computation Time			90ms (AHM)	19s (TDM)

Fig. 5 depicts the measured discharge pressures (left column) as a function of the angular position $\theta(t)$ in time domain and their ℓth harmonics $p_{d\ell}$ (right column), where $\ell = 1, \ldots, 5$ for the four operating speeds. The disturbance torque $\tau_p(\beta_0)$ and their corresponding ℓth harmonics ($\ell = 1, \ldots, 5$) computed from (A.2a) and (A2.b) are presented in the left and right columns of Fig. 6, respectively. For completeness, the steady-state values (β_0, τ_{p0}) and ($\boldsymbol{\tau}_{p\ell}$, $\mathbf{p}_{d\ell}$) at each operating speed are listed in Table II; only $\ell = 1, 2, 3$ components are included because the amplitudes of the higher order harmonics ($\ell = 4, 5$) are negligibly smaller than their fundamental components.

With known (τ_p, p_d) in terms of their steady-state values (τ_{p0}, p_{d0}) and HAVs ($\boldsymbol{\tau}_{p\ell}$, $\mathbf{p}_{d\ell}$), the computed β are compared with that experimentally measured in Fig. 7, both in time and frequency domains. The effects of the disturbance torque and feedback pressure on the HF SP oscillation are illustrated in Table III that compares their contributions characterized by ($\mathbf{G}\boldsymbol{\tau}_{p\ell}$, $\mathbf{H}\mathbf{p}_{d\ell}$) defined in (25a, b) for the four pump speeds.

The followings summarize the findings from the results.

1) As shown in Figs. 5 and 6, the measured discharge pressure p_d and computed disturbance torque $\tau_p(\beta_0)$ periodically fluctuate (with a period $2\pi/N$) about their steady-state values (p_{d0}, τ_{p0}) for all four speeds. As a result, the ℓth ($\ell = 1, 2, 3$) harmonics can be seen at the frequency $\ell N n_r/60$.
2) As compared in Fig. 6 and Table II (for identical p_{d0} and similar β_0), the waveforms (left) and harmonic amplitudes (right) of τ_p are almost the same under the four pump speeds, but those of the measured p_d vary with pump speeds.
3) As compared in Fig. 7 and Table III (last row), although both AHM and TDM predictions closely agree with that measured, the AHM took only 90ms to calculate the HF oscillations of a piston pump during one cycle, representing three orders less computation time than (or less than 0.5% of 19 s) that taken by the TDM. Some discrepancies are due to the neglected quadratic terms when deriving the AHM. The above results demonstrate that the AHM, which avoids highly repetitive integrations (required in TDM) in predicting the HF SP oscillations, is a computationally efficient model for real-time applications.
4) As shown in Fig. 7, the SP oscillates around its steady-state position β_0 (left column); and its HF oscillation is dominated by the fundamental component (right column). From the comparison between $\mathbf{G}\boldsymbol{\tau}_{p\ell}$ and $\mathbf{H}\mathbf{p}_{d\ell}$ in Table III, the HF oscillation is primarily contributed by the disturbance torque.
5) As shown in the zoom-in subplots of Figs. 5 and 6, there are low-frequency components in the discharge pressure and disturbance torque (at $\ell n_r/60$ where $\ell = 1, 2, 3$ and n_r is the pump operational speed), which vary with operating conditions. Their magnitudes are much smaller than that of the dominant HF components at $\ell N n_r/60$ ($N = 9$ is the piston number) but these low-frequency harmonics (unmodeled in AHM) contribute to some frequency shifts in the SP-angle oscillations; the discrepancy between predictions and measurements can be observed in Fig. 7 (left side), especially for the cases $n_r =$ (3600, 4200) r/min.

IV. Conclusion

A computationally efficient method to derive an AHM has been presented, where the AHM explicitly characterizes the harmonics of SP oscillations as a function of the feedback pressure ripples and pulsating external disturbance. Illustrated in the context of a PC system in an aircraft PC-PP, both the TDM and the AHM have been derived to characterize the SP oscillations under various operating speeds. The AHM has been evaluated by comparing its numerical solutions with experimental results; good agreements between simulations and experimental measurements validate the AHM method, and demonstrate its remarkable advantage for real time applications over conventional TDM methods. It is concluded that the HF SP oscillations under different operating speeds are dominated by their fundamental components; and that the disturbance torque is the main contributor on the HF SP oscillations. AHM provides a time-efficient alternative for modeling a noisy control system: Once the HAVs and 2×2 transfer matrices are derived; it can be used as a basis to analyze the periodic disturbance and/or feedback noises effects and design controllers to suppress undesired oscillations as illustrated in Appendix B.

Appendix

A. Calculations of Steady-State Values

For the PC-PP shown in Fig. 1 (where the parameters are defined in Table I), the equilibrium torques acting on the swashplate at any steady-state operating point (β_0, p_{d0}, ω_m) can be expressed as (A.1), where β_m is the maximum SP-angle

$$\tau_{p0}(\beta_0) + f_b l_a + k_b l_a^2(\beta_m - \beta_0) - p_{a0} A_a l_a = 0. \quad \text{(A.1)}$$

From (5a–c), (6a, b), (7b), and (1g), the steady-state value τ_{p0} of the disturbance torque τ_p along with the HAV $\boldsymbol{\tau}_{p\ell}$ and (I_{sa}, c_{sa}, b_{sa}) in (16) are derived in (A.2a–e) where $T_{\beta\gamma} = \tan\beta_0 \tan\gamma$, $S_{\beta_0} = \sin\beta_0$, $C_{\beta_0}^{-n} = (\cos\beta_0)^{-n}$ and $C_{\phi}^{-1} = (\cos\phi)^{-1}$

$$\frac{\tau_{p0}(\beta_0)}{N m_{ps} r_p^2 \omega_m^2} = \frac{\tan\beta_0}{2}\left(C_{\beta_0}^{-2} + \tan^2\gamma\right) + \frac{A_p p_0 a}{m_{ps} r_p^2 \omega_m^2}\left[C_{\beta_0}^{-2}\left(S_{\beta_0} C_{\phi}^{-1} - \frac{e}{a}\right) + \left[C_{\beta_0}^{-2} - T_{\beta\gamma}\right]\frac{\mathbf{p}_{n(k=1)}}{p_0 a}\right] \quad \text{(A.2a)}$$

$$\boldsymbol{\tau}_{p\ell}(\beta_0) = \frac{N A_p}{2} r_p \sum_{\pm}\left(\pm C_{\beta_0}^{-2}\mathbf{S} - T_{\beta\gamma}\mathbf{I}_{2\times 2}\right)\mathbf{p}_{n(k=\ell N\pm 1)} + a N A_p C_{\beta_0}^{-2}\left(S_{\beta_0} C_{\phi}^{-1} - \frac{e}{a}\right)\mathbf{p}_{n(k=\ell N)} \quad \text{(A.2b)}$$

$$\frac{I_{sa}(\beta_0)}{N m_{ps} r_p^2} = \frac{C_{\beta_0}^{-4}}{2}\left[1 + 2\frac{a^2}{r_p^2}\left(S_{\beta_0} C_{\phi}^{-1} - \frac{e}{a}\right)\left(S_{\beta_0} - \frac{e}{a}\right)\right] \quad \text{(A.2c)}$$

$$\frac{c_{sa}(\beta_0)}{N m_{ps} r_p^2} = S_{\beta_0} C_{\beta_0}^{-5} \times\left[1 + \frac{a^2}{r_p^2}\left(S_{\beta_0} C_{\phi}^{-1} - \frac{e}{a}\right)\left(S_{\beta_0}^{-1} - \frac{2e}{a} + S_{\beta_0}\right)\right] \quad \text{(A.2d)}$$

$$\frac{b_{sa}(\beta_0)}{N m_{ps} r_p^2} = -\omega_m T_{\beta\gamma} C_{\beta_0}^{-2}. \quad \text{(A.2e)}$$

In (A.2a), $\mathbf{p}_{nk}$ has been defined in (15b), the steady-state value p_0 of the nth piston chamber pressure p_n can be directly obtained from the Fourier Transform of the pressure profile [see Fig. 1(a)] as given in the following equation:

$$p_0 = p_s + (p_{d0} - p_s)(\varphi_{fe} + \varphi_{fs} - \varphi_{rs} - \varphi_{re})/4\pi. \quad \text{(A.2f)}$$

As indicated in (A.2a, b), the reciprocating inertial force of the piston/slipper assemblies increases with ω_m^2 contributing to a growing average torque $\tau_{p0}(\beta)$, while $\boldsymbol{\tau}_{p\ell}(\beta)$ is independent of ω_m with given $\mathbf{p}_{nk}$.

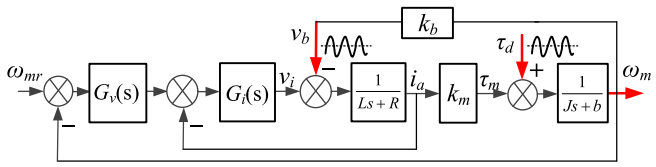

Fig. 8. Speed control system with noisy load and back emf [27].

Given $(\beta_0, p_{d0}, \omega_m)$ and the pump parameters, the steady-state value p_{a0} determined from (A.1) provides a basis to calculate the remaining steady-state values in the hydraulic circuit (see Fig. 2)

$$q_{10} = q_{(3+)0} = q_{v0} = q_{70} = q_{a0} = c_{la}(p_{a0} - p_c) \quad \text{(A.3a)}$$

$$p_{20} = p_{d0} - q_{10}R_1; \quad p_{(4-)0} = p_c \quad \text{(A.3b-c)}$$

$$p_{(4+)0} = p_{20} - q_{(3+)0}R_{3+}; p_{60} = p_{a0} + (R_7 + R_9)\, q_{a0} \quad \text{(A.3d-e)}$$

$$k_v x_{v0} = (p_{20} - p_c)\, A_{v1} + \left(p_{(4+)0} - p_{(4-)0}\right) A_{v2} - f_r. \quad \text{(A.3f)}$$

Note that the valve displacement x_{v0} is positive introducing the oil from the discharge port to compensate the leakage flowrate q_{a0} to the reservoir p_c. Thus, $q_{(3+)0} = q_{v0}$ in (A.3a), and the steady state $p_{(4-)0} = p_c$.

B. Illustrative AHM Applications

Consider the noisy speed control system in Fig. 8, where (J, b) are the (moment of inertia, viscous damping coefficient) of the rotating system; (L_a, R_a) are the (inductance, resistance) of the motor windings with current i_a and input voltage v_i; and $k_m\,(= \tau_m/i_a)$ of the motor-torque constant. AHM is used to identify periodic disturbance torque τ_d and back electromotive-force (back emf $v_b = k_b\omega_m$ as internal feedback) for designing the speed and current controllers, $G_v(s)$ and $G_i(s)$, to suppress speed ripple ω_m with respect to the reference ω_{mr} [27]. Using the definitions (1a–c), the HAVs $(\mathbf{v}_{i\ell}, \mathbf{v}_{b\ell}, \mathbf{i}_{a\ell}, \boldsymbol{\tau}_{d\ell}, \boldsymbol{\omega}_{m\ell})$ of the incremental variables $(v_i, v_b, i_a, \tau_d, \omega_m)$ can be derived

$$\mathbf{v}_{i\ell} = -\mathbf{G}_i\left(\mathbf{G}_v\boldsymbol{\omega}_{m\ell} + \mathbf{i}_{a\ell}\right);$$

$$\mathbf{v}_{i\ell} - \mathbf{v}_{b\ell} = \left(\ell\omega L_a\mathbf{S} + R_a\mathbf{I}\right)\mathbf{i}_{a\ell} \quad \text{(B.1a-b)}$$

$$\left(\ell\omega J\mathbf{S} + b\mathbf{I}\right)\boldsymbol{\omega}_{m\ell} = k_m\mathbf{i}_{a\ell} + \boldsymbol{\tau}_{d\ell}. \quad \text{(B.1c)}$$

In (B.1a), $(\mathbf{G}_v, \mathbf{G}_i)$ are the 2×2 transfer-function matrices of the speed and current controllers respectively. Consider the commonly used proportional–integral–differential controller with parameters (K_p, T_i, T_d) as an illustrative example in (B.2a), its transfer-function matrix $\mathbf{G}_c$ has the form in (B.2b)

$$G_c(s) = K_p\left(1 + 1/T_i s + T_d s\right) \quad \text{(B.2a)}$$

$$\mathbf{G}_c = K_p\left(\mathbf{S}^{-1}/\ell\omega T_i\right)\left[\left(1 - \ell^2\omega^2 T_i T_d\right)\mathbf{I} + \ell\omega T_i\mathbf{S}\right]. \quad \text{(B.2b)}$$

Eliminating $\mathbf{v}_{i\ell}$ and $\mathbf{i}_{a\ell}$ from (B.1a–c), the AHM for the noisy speed control system (see Fig. 8) can be derived as follows:

$$\boldsymbol{\omega}_{m\ell} = \mathbf{H}^{-1}\left(\mathbf{G}_\tau\boldsymbol{\tau}_{d\ell} - k_m\mathbf{v}_{b\ell}\right) \quad \text{(B.3a)}$$

where $\mathbf{G}_\tau = \mathbf{G}_i + \ell\omega L_a\mathbf{S} + R_a\mathbf{I}$; and (B.3b)

$$\mathbf{H} = k_m\mathbf{G}_i\mathbf{G}_v + \mathbf{G}_\tau\left(\ell\omega J\mathbf{S} + b\mathbf{I}\right). \quad \text{(B.3c)}$$

With known operating frequencies $\ell\omega$ and parameters (J, b, L_a, R_a), AHM (B.3a–c) with the 2×2 transfer matrices $(\mathbf{H}, \mathbf{G}_\tau)$ can be used as constraints to design (G_v, G_i) to suppress ripples (for example, proportion-integral-resonant controller [27]), and estimate the effects of the unknown disturbance torque in real-time if the back emf v_b and speed ripple ω_m can be monitored.

REFERENCES

[1] H. Muramatsu and S. Katsura, "Adaptive periodic-disturbance observer for periodic-disturbance suppression," *IEEE Trans. Ind. Informat.*, vol. 14, no. 10, pp. 4446–4456, Oct. 2018.

[2] J. Yao, Z. Jiao, and D. Ma, "A practical nonlinear adaptive control of hydraulic servomechanisms with periodic-like disturbances," *IEEE/ASME Trans. Mech.*, vol. 20, no. 6, pp. 2752–2760, Dec. 2015.

[3] K.-M. Lee, L. Li, K. Bai, X. Ouyang, and H. Yang, "Harmonic model and remedy strategy of multiphase PM motor under open-circuit fault," *IEEE/ASME Trans. Mech.*, vol. 24, no. 3, pp. 1407–1419, Mar. 2019.

[4] P. Cui, S. Li, G. Zhao, and C. Peng, "Suppression of harmonic current in active–passive magnetically suspended CMG using improved repetitive controller," *IEEE/ASME Trans. Mech.*, vol. 21, no. 4, pp. 2132–2141, Aug. 2016.

[5] X. Huo, M. Wang, L. K.-Z. Liu, and X. Tong, "Attenuation of position-dependent periodic disturbance for rotary machines by improved spatial repetitive control with frequency alignment," *IEEE/ASME Trans. Mech.*, vol. 25, no. 1, pp. 339–348, Feb. 2020.

[6] G. Liu, B. Chen, K. Wang, and X. Song, "Selective current harmonic suppression for high-speed PMSM based on high-precision harmonic detection method," *IEEE Trans. Ind. Informat.*, vol. 15, no. 6, pp. 3457–3468, Jun. 2019.

[7] L. Li, "Research on the dynamic characterisitics of high speed motor-pump unit," Ph.D. dissertation, Dept. Mech. Eng., Zhejiang Univ., Hangzhou, China, 2019.

[8] W. Kemmetmüller, F. Fuchshumer, and A. Kugi, "Nonlinear pressure control of self-supplied variable displacement axial piston pumps," *Control Eng. Pract.*, vol. 18, no. 1, pp. 84–93, Jan. 2010.

[9] J. Koivumäki and J. Mattila, "Adaptive and nonlinear control of discharge pressure for variable displacement axial piston pumps," *ASME J. Dyn. Syst. Meas. Control*, vol. 139, no. 10, Oct. 2017, Art. no. 101008.

[10] L. Li, K.-M. Lee, X. Ouyang, and H. Yang, "Attenuating characteristics of a multi-element buffer bottle in an aircraft piston pump," *Proc. Inst. Mech. Eng., Part C*, vol. 231, no. 10, pp. 1791–1803, May 2017.

[11] J.-H. Shin, "Computational study on dynamic pressure in a swash-plate axial piston pump connected to a hydraulic line with an end resistance," *J. Mech. Sci. Technol.*, vol. 29, no. 6, pp. 2381–2390, Dec. 2015.

[12] S. Wang, "Generic modeling and control of an open-circuit piston pump—Part I: theoretical model and analysis," *ASME J. Dyn. Syst., Meas., Control*, vol. 138, no. 4, Apr. 2016, Art. no. 041004.

[13] L. Ericson, "Swash plate oscillations due to piston forces in variable in-line pumps," in *Proc. Int. Fluid Power Conf.*, 2014, pp. 217–225.

[14] G. K. Seeniraj and M. Ivantysynova, "Impact of valve plate design on noise, volumetric efficiency and control effort in an axial piston pump," in *Proc. ASME Int. Mech. Eng. Cong. Expo.*, 2006, pp. 77–84.

[15] P. Achten, "Dynamic high-frequency behaviour of the swash plate in a variable displacement axial piston pump," *Proc. Inst. Mech. Eng., Part I*, vol. 227, no. 6, pp. 529–540, Jun. 2013.

[16] X. Fang, X. Ouyang, and H. Yang, "Investigation into the effects of the variable displacement mechanism on swash plate oscillation in high- speed piston pumps," *Appl. Sci.*, vol. 8, no. 5, pp. 2076–3417, Apr. 2018.

[17] T. Kim and M. Ivantysynova, "Active vibration control of swash plate- type axial piston machines with two-weight notch least mean square/ filtered-x least mean square filters," *Energies*, vol. 10, no. 5, 2017, Art. no. 645.

[18] J. Lux and H. Murrenhoff, "Experimental loss analysis of displacement controlled pumps," in *Proc. Int. Fluid Power Conf.*, 2016, pp. 441–452.

[19] J. W. Dobchuk, "Sub-component level modeling of a variable displacement axial piston pump," Ph.D. dissertation, Dept. Mech. Eng., Univ. Saskatchewan, Saskatoon, SK, Canada, 2000.

[20] M. K. Bahr, J. Svoboda, and R. B. Bhat, "Vibration analysis of constant power regulated swash plate axial piston pumps," *J. Sound Vib.*, vol. 259, no. 5, pp. 1225–1236, Jan. 2003.
[21] P. A. J. Achten, S. Eggenkamp, and H. W. Potma, "Swash plate oscillation in a variable displacement floating cup pump," in *Proc. 13th Scand. Int. Conf. Fluid Power*, 2013, pp. 163–176.
[22] L. Li, K.-M. Lee, K. Bai, X. Ouyang, and H. Yang, "Inverse models and harmonics compensation for suppressing torque ripples of multiphase permanent magnet motor," *IEEE Trans. Ind. Electron.*, vol. 65, no. 11, pp. 8730–8739, Nov. 2018.
[23] N. D. Manring, "Designing a control and containment device for cradle-mounted, transverse-actuated swash plates," *ASME J. Mech. Des.*, vol. 123, no. 3, pp. 447–455, Sep. 2001.
[24] N. D. Manring and Z. Dong, "The impact of using a secondary swash-plate angle within an axial piston pump," *ASME J. Dyn. Syst., Meas., Control*, vol. 126, no. 1, pp. 65–74, Mar. 2004.
[25] A. Johansson, J. Övander, and J. O. Palmberg, "Experimental verification of cross-angle for noise reduction in hydraulic piston pumps," *Proc. Inst. Mech. Eng., Part I*, vol. 221, no. 3, pp. 321–330, May 2007.
[26] S. Wang, "Novel piston pressure carryover for dynamic analysis and designs of the axial piston pump," *ASME J. Dyn. Syst., Meas., Control*, vol. 135, no. 2, 2013, Art. no. 024504.
[27] C. Xia, B. Ji, and Y. Yan, "Smooth-speed control for low speed high torque permanent magnet synchronous motor using proportional intergral resonant controller," *IEEE Trans. Ind. Electron.*, vol. 62, no. 4, pp. 2123–2134, Apr. 2015.

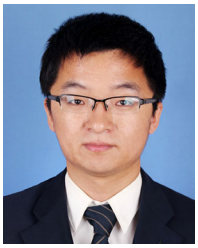

Lei Li received the B.S. degree from Tianjin University, Tianjin, China, in 2012, and the Ph.D. degree from Zhejiang University, Hangzhou, China, in 2019, both in mechanical engineering.

He was a Visiting Scholar with the Woodruff School of Mechanical Engineering, Georgia Institute of Technology, Atlanta, GA, USA, during 2016–2017. He is currently an Algorithm Engineer with the B&R Industrial Automation @ ABB group. His research interests include dynamics/control and mechatronics.

Kok-Meng Lee (Fellow, IEEE) received the B.S. degree from the State University of New York, Buffalo, NY, USA, in 1980, and the S.M. and Ph.D. degrees from the Massachusetts Institute of Technology, Cambridge, MA, USA, in 1982 and 1985, respectively, all in mechanical engineering.

He is currently a Professor with the George W. Woodruff School of Mechanical Engineering, Georgia Institute of Technology, Atlanta, GA, USA. His research interests include system dynamics/control, robotics, automation, and mechatronics.

Dr. Lee is a Life Fellow of the American Society of Mechanical Engineers. He is the founding Editor-in-Chief for the *Springer International Journal of Intelligent Robotics and Applications*. He served as the Editor-in-Chief for IEEE/ASME TRANSACTIONS ON MECHATRONICS (2008–2013). He was the recipient of the National Science Foundation Presidential Young Investigator, Woodruff Faculty Fellow, Sigma Xi Junior Faculty Research, International Hall of Fame New Technology, Kayamori Best Paper and Michael J. Rabins Leadership Awards.

Xiaoping Ouyang received the B.S. and M.S. degrees from Northeast Petroleum University, Anda, China, in 1997 and 2000, respectively, and the Ph.D. degree from Zhejiang University, Hangzhou, China, in 2005, all in mechanical engineering.

He is currently a Professor with the State Key Laboratory of Fluid Power and Mechatronic Systems, Zhejiang University. His research interests include electrohydraulic system control, aircraft hydraulics, and exoskeleton robots.

Huayong Yang received the B.S. degree from the Huazhong University of Science and Technology, Wuhan, China, in 1982, and the Ph.D. degree from the University of Bath, Bath, U.K., in 1988, both in mechanical engineering.

Since 1989, he has been with Zhejiang University, Hangzhou, China, where he is the Director of the State Key Laboratory of Fluid Power and Mechatronic Systems and the Department of Mechanical Engineering. His current research interests include motion control and energy saving of mechatronic systems, fluid power components, and system development.

Dr. Yang is an Academician of the Chinese Academy of Engineering. He was the recipient of the first class of the National Scientific and Technological Progress Award, the National Outstanding Researcher of the Natural Science Foundation of China, and three Ministerial or Provincial Scientific and Technological Progress Prizes.